Progress In Electromagnetics Research M, Vol. 117, 37–46, 2023

A New Compressive Sensing Method for Speckle Reducing in Complex-Valued SAR Data

Nabil Gherbi[1, *], Azzedine Bouaraba[1], Mustapha Benssalah[2], and Aichouche Belhadj Aissa[3]

Abstract—High resolution Synthetic Aperture Radar (SAR) images are affected by speckle noise, which considerably reduces their visibility and complicates the target identification. In this paper, a new Compressive Sensing (CS) method is proposed to reduce the speckle noise effects of complex valued SAR images. The sparsity of the SAR images allows solving the CS problem using Multiple Measurements Vector (MMV) configuration. Therefore, a special weighted norm is constructed to solve the optimization problem, so that the Variance-Based Joint Sparsity (VBJS) model is used to calculate the weights. An efficient Alternating Direction Method of Multipliers (ADMM) is developed to solve the optimization problem. The obtained results using raw complex-valued measurements with ground truth demonstrate the effectiveness of the proposed despeckling method in terms of both image quality and computational cost.

1. INTRODUCTION

Synthetic Aperture Radar (SAR) system is an important remote sensing tool capable of generating high resolution images of ground targets [1, 2]. However, the so-called speckle which is a multiplicative-noise-like phenomenon highly affects the acquired SAR images [3]. Considerable importance is given to speckle reduction, by exploiting many algorithms to preserve the final image resolution as much as possible. Among these algorithms, many classical filters have been widely applied, including: Lee [4], Kuan et al. [5], Frost et al. [6], and the Gamma Maximum A Posteriori (MAP) filter [7, 8]. Furthermore, the Multiplicative Image Despeckling by Augmented Lagrangian (MIDAL) [9] and the Patch Ordering-based via Transform-Domain [10] filters (POTDFs) have been applied to improve the filtering robustness. Recently, Compressive Sensing (CS) algorithms have been successfully applied to SAR images despeckling and reconstruction [11, 12]. SAR image usually exhibits sparsity in terms of such features, which motivates the SAR model formulation as a CS problem.

CS-based methods are mostly considered in the literature as an inverse problem. The matrix formulation is employed, which unfortunately requires large computational resources. Therefore, the sparsity of SAR scenes with multi-frequency points encourages the formulation of the CS problem in a Multiple Measurements Vector (MMV) setup [13]. MMV is an extension of single measurements vector, which deals with the restoration of sparse signal vectors having a common support. In [14], MMV methodology is investigated to estimate the reflectivity matrix by assuming that the scatterers are represented in the row support of the image domain, and the columns represent the different values of reflectivity corresponding to the frequency band, polarization, and sub-aperture. It has been shown in [15] that the reconstruction can be achieved by considering a general l_p-norm minimization. However,

Received 15 November 2022, Accepted 12 May 2023, Scheduled 19 May 2023
* Corresponding author: Nabil Gherbi (gherbi.nabil.81@gmail.com).
[1] Laboratoire Radar, Ecole Militaire Polytechnique, BP 17, 16111, Bordj-El-Bahri, Algiers, Algeria. [2] Laboratoire Traitement de Signal, Ecole Militaire Polytechnique, BP 17, 16111, Bordj-El-Bahri, Algiers, Algeria. [3] Image Processing and Radiation Laboratory, University of Sciences and Technology Houari Boumediene, USTHB, Algeria.

optimal recovery of the sparse images requires an Nondeterministic Polynomial (NP)-complex l_0-norm minimization problem. Therefore, great importance has been given to construct an efficient group sparse regularization as in [16], where the authors proposed an $l_{1/2,1}$ regularization to overcome the shortcomings of the $l_{1,2}$ and $l_{1,\infty}$ in a CS framework. Recently, the Variance Based Joint Sparsity (VBJS) has been investigated in many reconstruction problems [17, 18].

This paper proposes a new CS-based algorithm by considering the MMV model. The minimization problem is formulated using an iterative re-weighted mixed $l_{2,1}$-norm. The weights are calculated as in [18] by considering the variance information between multiple measurements. The optimization problem is solved using the Alternating Direction Method of Multipliers (ADMM) [19].

The rest of this paper is organized as follows. Section 2 gives the problem modeling. Section 3 is devoted to the experimental setup. Section 4 presents the obtained results. Section 5 concludes the paper.

2. PROBLEM MODELING

The observation model for a SAR imaging system can be expressed as

$$Y = \Psi X + B \tag{1}$$

where $Y \in \mathbb{C}^{ZR\times 1}$, $\Psi \in \mathbb{C}^{ZR\times MN}$, $X \in \mathbb{C}^{MN\times 1}$, $B \in \mathbb{C}^{ZR\times 1}$. Y is the radar backscattered signal, Ψ the observation matrix, X the reflectivity, B the system noise, MN the size of the imaged scene, and Z, R are the number of azimuth and range samples, respectively.

The reflectivity X for SAR image can be written as

$$X = \sqrt{x} \odot n \tag{2}$$

where $\sqrt{x}$ is the SAR image amplitude, $n \in \mathbb{C}^{MN\times 1}$ the speckle noise, and $\odot$ the element-wise multiplication.

The speckle intensity can be modeled by a Gamma distribution as follows

$$p_n(n) = L^L \frac{1}{\Gamma(L)}\, n^{L-1} \exp(-Ln) \tag{3}$$

where L is the number of looks.

In the CS framework, the radar backscattered signal Y is compressed with a matrix $\Phi \in \mathbb{C}^{ZR\times s}$, with $s \ll MN$. So Equation (1) can be rewritten as follows

$$Y = \Phi\Psi X + B \tag{4}$$

The matrix $A = \Phi\Psi$ satisfies the Restricted Isometry Property (RIP) conditions, and the SAR scene is sparse, so the unknown reflectivity can be recovered using l_1-norm regularization by solving the following optimization problem

$$\min_X \|AX - Y\|_F^2 + \alpha \|X\|_1 \tag{5}$$

where α is a sparsity balancing term.

As the SAR data is arranged in a matrix, the rows of the unknown reflectivity X correspond to the scatterers positions and the columns to the measurements. Since the scene is sparse, the problem can be formulated as an MMV joint sparse recovery.

In this work, the mixed $l_{2,1}$-norm instead of l_1-norm is proposed, and the new problem formulation can be expressed as

$$\min_X \|AX - Y\|_F^2 + \alpha \|X\|_{2,1} \tag{6}$$

In [20], a log-sum penalty is used to relax the l_0-norm to overcome the l_1 penalty problem, where the large magnitudes are highly penalized compared to small ones. Equation (6) can be expressed as

$$\begin{aligned} &\min_X \|AX - Y\|_F^2 + \alpha \sum_{i=1}^{N} \log(z_i + \varepsilon) \\ &\text{s.t } \|x_i\|_2 \le z_i,\ \forall i \in \mathbb{N} \end{aligned} \tag{7}$$

The log term is concave and can be approximated by its first Taylor expansion using the Majorization Minimization (MM) approach [21]. For that, an iteratively re-weighted formulation of the optimization problem is given by

$$X^{(t+1)} = \min_{X} \|AX - Y\|_F^2 + \alpha \sum_{i=1}^{N} w_i^{(t)} \|x_i\|_2 \tag{8}$$

where $w^{(t)}$ denotes the vector of weights at the (t)th MM iteration. The vector w is evaluated as in [18] by taking into account the variance information between multiple measurements.

2.1. VBJS Weights Formulation

The variance vector is given as follows

$$\upsilon_i = \frac{1}{J} \sum_{j=1}^{J} P_{i,j}^2 - \left(\frac{1}{J} \sum_{j=1}^{J} P_{i,j} \right)^2 \tag{9}$$

where J is the number of measurements and P the vector containing the sparsity information of all measurements represented by

$$P = \left[TX^{(1)}\ TX^{(2)}\ ...\ TX^{(J)} \right] \tag{10}$$

The transform T, defined by a Polynomial Annihilation (PA) operator [22], has been used to approximate the sparse image domain. By normalizing the magnitudes of each column's vector elements in matrix P, the vector form can be expressed as follows

$$\tilde{P}_{i,j} = \frac{|P_{i,j}|}{\max |P_{i,j}|}, \quad j = 1, ..., J,\ i = 1, ..., N \tag{11}$$

A scalar weighting is defined and constructed by averaging the l_1-norm of each P column to avoid the manual tuning of parameters. It can be written as

$$C = \frac{1}{J} \sum_{j=1}^{J} \sum_{i=1}^{N} \tilde{P}_{i,j} \tag{12}$$

The weight vector can be calculated using Equations (9), (11), and (12) as

$$w_i = \begin{cases} C \left(1 - \dfrac{\upsilon_i}{\max \upsilon_i} \right), & i \notin I \\ \dfrac{1}{C} \left(1 - \dfrac{\upsilon_i}{\max \upsilon_i} \right), & i \in I \end{cases} \tag{13}$$

The interval I is selected by comparing the normalized vector mean of measurements $\tilde{P}$ over all measurements J with a threshold τ, which depends on the noise level as follows

$$\frac{1}{J} \sum_{j=1}^{J} \tilde{P}_{i,j} \succ \tau \tag{14}$$

2.2. ADMM Solution

The optimization problem in Equation (8) is solved by an ADMM algorithm. The augmented Lagrangian of Equation (8) can be written as follows

$$\min_{X,Z} \alpha \sum_{i=1}^{N} w_i^{(t)} \|x_i\|_2 + \|AZ - Y\|_F^2 + \frac{\rho}{2} \left\| X - Z + \frac{\lambda}{\rho} \right\|_F^2 - \frac{\|\lambda\|_F^2}{2\rho} \tag{15}$$

The auxiliary variable $Z \in \mathbb{C}^{MN}$ and Lagrange multiplier $\lambda \in \mathbb{C}^{MN}$ are introduced in the Lagrangian formulation. The positive parameter ρ is used to penalize the Frobenius norm quadratic terms.

The ADMM iteration is used to minimize the Lagrangian in (15) with respect to the X, Z, and the updates of the Lagrange multiplier λ are given by the following equations (with k denotes the ADMM iteration index).

$$\begin{cases} Z^{(k+1)} = \min\limits_{Z} L\left(Z, X^{(k)}, \lambda^{(k)}\right) \\ X^{(k+1)} = \min\limits_{X} L\left(Z^{(k+1)}, X, \lambda^{(k)}\right) \\ \lambda^{(k+1)} = \lambda^{(k)} + \rho\left(X^{(k+1)} - Z^{(k+1)}\right) \end{cases}$$

The optimization problem can be performed by separately solving the following sub-problems.

2.2.1. Z-Subproblem

Fixing $X^{(k)}$ and $\lambda^{(k)}$, Equation (15) can be transformed into

$$Z^{(k+1)} = \min_{Z} \|AZ - Y\|_F^2 + \frac{\rho}{2}\left\|X^{(k)} - Z + \frac{\lambda^{(k)}}{\rho}\right\|_F^2 \tag{16}$$

Since the objective function of Z is strictly convex, Equation (16) has a unique solution obtained by calculating the gradient with respect to Z and setting the result to zero

$$Z^{(k+1)} = \left(A^T A^* + \rho I_N\right)^{-1}\left(\rho X^{(k)} + \lambda^{(k)} + Y^T A^*\right) \tag{17}$$

where $(\cdot)^T$ and $(\cdot)^*$ denote the transpose and complex conjugate operators, respectively.

2.2.2. X-Subproblem

Fixing $Z^{(k+1)}$ and $\lambda^{(k)}$, Equation (15) can be transformed into

$$X^{(k+1)} = \min_{X} \alpha \sum_{i=1}^{N} w_i^{(t)} \|x_i\|_2 + \frac{\rho}{2}\left\|X - Z^{(k+1)} + \frac{\lambda^{(k)}}{\rho}\right\|_F^2 \tag{18}$$

The values of X in Equation (18) can be updated by splitting the problem into N sub-problems

$$x_i^{(k+1)} = \min_{x_i} \frac{\alpha w_i^{(t)}}{\rho} \|x_i\|_2 + \frac{1}{2}\left\|x_i - z_i^{(k+1)} + \frac{\lambda_i^{(k)}}{\rho}\right\|_2^2 \tag{19}$$

The X sub-problem admits a closed-form solution. In particular, this solution is given by the shrinkage operator [23] as follows

$$x_i^{(k+1)} = \max\left\{\left\|z_i^{(k+1)} - \frac{\lambda_i^{(k)}}{\rho}\right\|_2 - \frac{\alpha w_i^{(t)}}{\rho}, 0\right\} \times \frac{z_i^{(k+1)} - \dfrac{\lambda_i^{(k)}}{\rho}}{\left\|z_i^{(k+1)} - \dfrac{\lambda_i^{(k)}}{\rho}\right\|_2} \tag{20}$$

Finally, the Lagrange multiplier λ is updated as follows:

$$\lambda^{(k+1)} = \lambda^{(k)} + \rho\left(X^{(k+1)} - Z^{(K+1)}\right) \tag{21}$$

The details to solve the ADMM solution are given by Algorithm 1.

Algorithm 1: Proposed Algorithm.

Input: α, ρ, τ, t_{max}, k_{max}, ϵ.
Output: $X^{(0)}$, $Z^{(0)}$, λ.
Initialization: $k = 1$, $t = 1$.
repeat
  for $t < t_{max}$ **do**
    for $k < k_{max}$ **do**
      $*$ Update $Z^{(k+1)}$ using 17
      $*$ Update $X^{(k+1)}$ using 20
      $*$ Update λ^{k+1} using 21
      $k \leftarrow k + 1$
    $X^{(l)} \leftarrow X^{(k+1)}$
    Calculate w_i using 13
until $\left\|X^{(k)} - X^{(k-1)}\right\|_F^2 < \epsilon$;

3. EXPERIMENTAL SETUP

The experimental setup shown in Figure 1 has been realized at the Radar Laboratory of the Military Polytechnic School of Algeria. The system configuration consists of a Vector Network Analyzer (VNA) operating within X band (8–12 GHz) and generates stepped frequency continuous wave signals. The VNA is connected to the transmitting-receiving patch antennas, which are felted by an angle of 45° toward the imaged scene. The antennas are positioned at a height of 1.35 m, which move in the cross-range direction using rail scanner with a step of 1.5 cm. For all the 61 equally spaced positions, the phase history data is collected. The quality of the despeckled SAR image is measured using the Peak Signal to Noise Ratio (PSNR) with different values of PA operator order. For this purpose, the robustness of the filtering process was analyzed through the variation of the PA operator. As shown in Figure 2, PA = 3 provides the maximum PSNR for the minimum number of iterations. This value is used in our despeckling process.

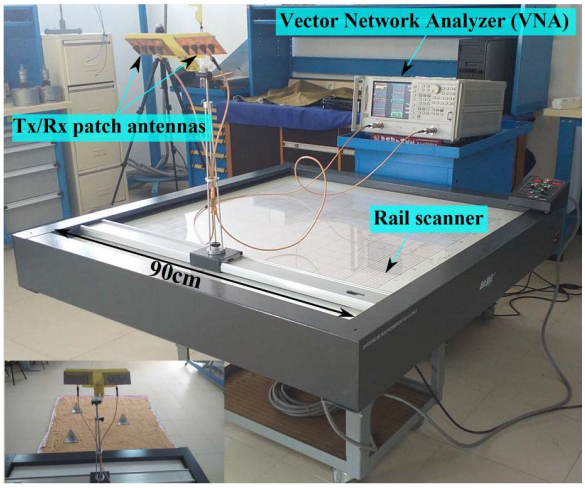

Figure 1. Experimental setup.

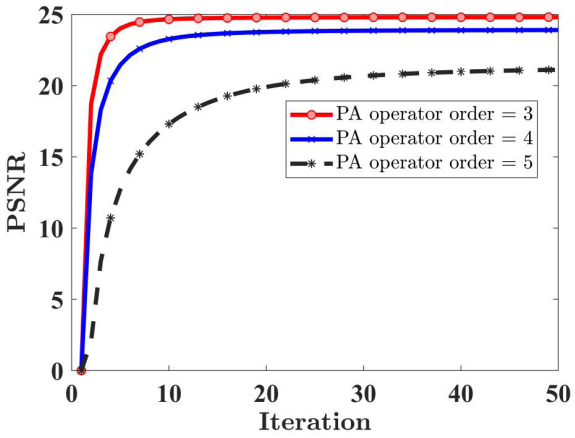

Figure 2. PSNR for different values of PA operator order.

For CS parameters, a random frequency sampling is performed for each cross-range position to reduce the amount of data processing. For the two conducted experiments, 240 frequency bins are taken out of 1602, which corresponds to approximately only 15% of the total frequency bins. Moreover, the sparsity balancing term α is set to 7×10^{-3} for the first experiment and 10^{-3} for the second one.

4. EXPERIMENTAL RESULTS

To demonstrate the despeckling accuracy of the proposed algorithm, the results of two experiments are summarized in this section.

4.1. First Experiment

Figure 3 shows the first imaged scene composed by a layer of sand with five identical corner reflectors. Figure 3(c) shows the obtained result using the Time Domain Back-projection Algorithm TDBPA [24]. It can be seen that the corner reflectors responses are dominant causing a strong interference and a visible speckle noise distributed in the entire surface. Figure 3(d) shows that the reconstructed image using the proposed algorithm is noiseless while the high resolution is presented. Moreover, all the targets are successfully reconstructed in their exact positions.

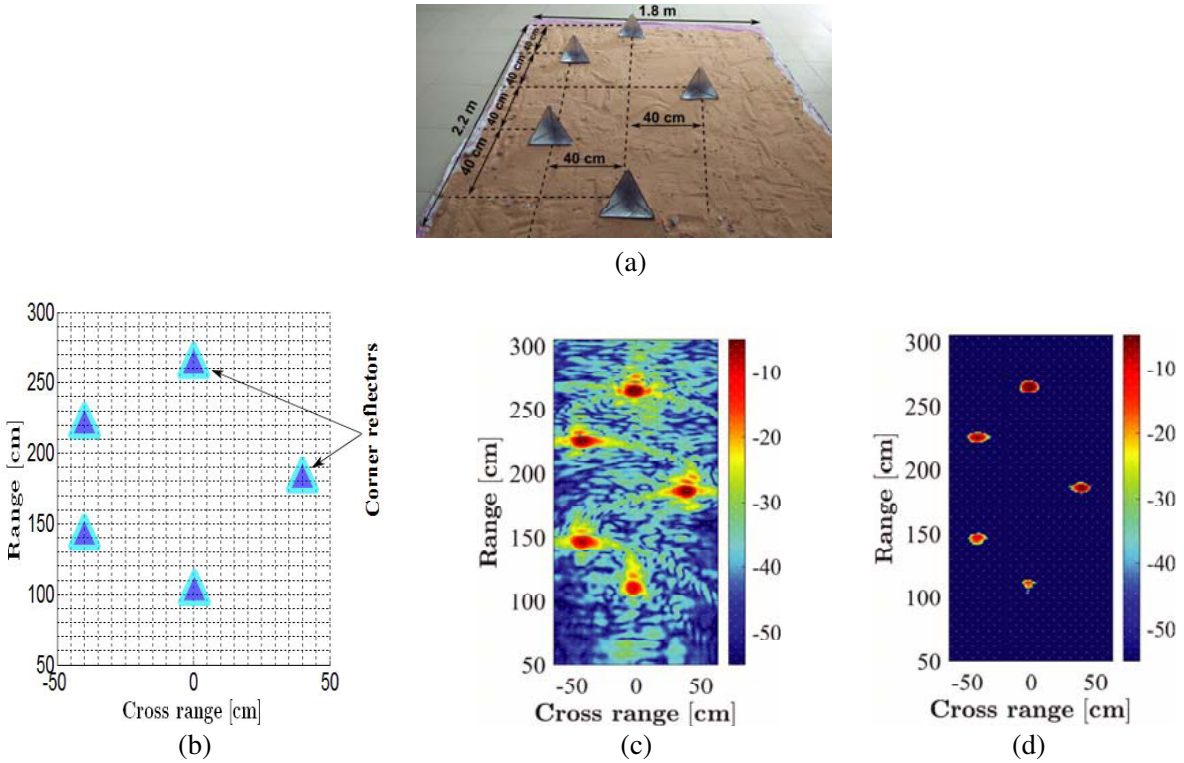

Figure 3. (a) First imaged scene. (b) Geometrical illustration of the scene. (c) Focused image by TDBPA. (d) Reconstructed image by the proposed algorithm.

4.2. Second Experiment

In this experiment, as shown in Figure 4, other targets are introduced with different radar cross section values. It can be observed in Figure 4(c) that the four dominant corner reflectors create a strong interferences which almost covers the other targets. The reconstructed image by the proposed method in Figure 4(d) shows that all targets are successfully recovered from noise, despite the weak radar

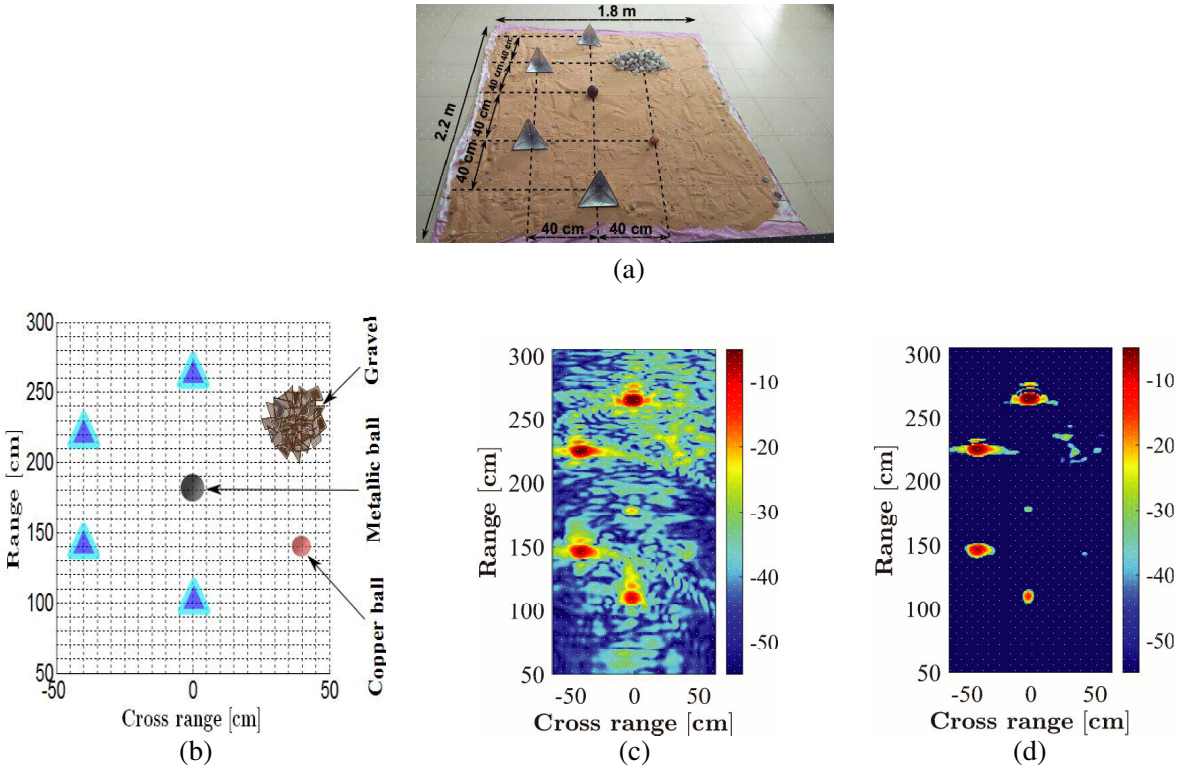

Figure 4. (a) Second imaged scene. (b) Geometrical illustration of the scene. (c) Focused image by TDBPA. (d) Reconstructed image by the proposed algorithm.

backscattering of the gravel surface and the two metallic balls. The introduced variance based weights w_i have perfectly contributed to the low-intensity edges restoration while reducing considerably the speckle.

4.3. Comparative Study

The second experiment is selected to perform the comparison with the following filtering algorithms: Kuan [5], Frost [6], MIDAL [9], and POTDF [10]. The despeckling results are obtained with selecting the best parameters for each algorithm as shown in Figure 5. It can be seen by visual perception in Figures 5(b) and 5(e) that Kuan and POTDF filters over-smooth both speckle noise and targets signals.

Moreover, resulting edges and contours are blurred and not well preserved. However, Frost and MIDAL filters (Figures 5(c) and 5(d)) perform better and provide more sharp edges. Figure 5(f) shows that our proposed algorithm efficiently suppress speckle noise while maintaining all the imaged targets.

Table 1. Quantitative metrics of despeckling methods applied to the second imaged scene.

	Parameters			
Method	ENL	SSIM	PSNR	RMSE
Kuan	0.24	0.21	18.92	1.68
Frost	0.52	0.47	22.30	1.41
MIDAL	0.46	0.39	20.23	1.51
POTDF	0.28	0.23	19.20	1.62
Proposed	**2.82**	**0.75**	**24.98**	**1.26**

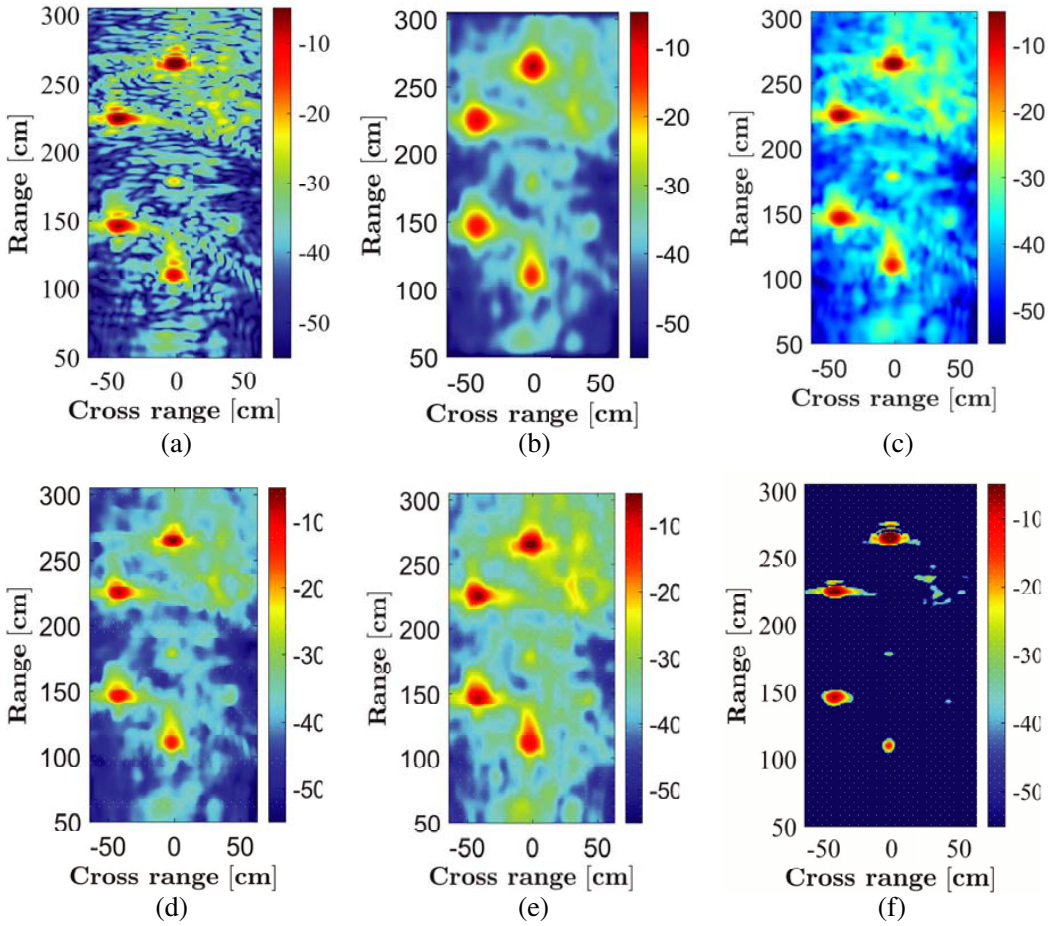

Figure 5. Despeckling results of second experiment. (a) Focused image by TDBPA, (b) Kuan, (c) Frost, (d) MIDAL, (e) POTDF, (f) proposed.

Table 2. ISLR values of the second imaged scene.

	Full data (100%)	45% of data	35% of data	15% of data
ISLR [dB]	−32.21	−30.52	−28.22	−17.65

The obtained results are evaluated using diverse quantitative metrics: Equivalent Number of Looks (ENL), Structural Similarity Index (SSIM), PSNR, and Root Mean Square Error (RMSE) [25]. According to Table 1, the best ENL value is achieved by our algorithm showing both high speckle reduction capability and radiation characteristics preservation. Note that the original noisy image has an ENL = 0.16. Our method outperforms the other methods in terms of SSIM which measures the similarity between the filtered image and the original one. Moreover, our algorithm provides higher PSNR value (equivalently, lower RMSE), which means better speckle reduction. Another criterion which is the integrated side lobe ratio (ISLR) is exploited to assess the effectiveness of CS based imaging algorithm. ISLR can be described by the ability of side lobe suppression which is defined as the ratio of the power (or energy) in the main peak to the total power in all side lobes [26]. In Table 2, the ISLR is calculated for different values of frequency sampled data. The best result is achieved for the measurements which correspond to 15% of the whole data.

5. CONCLUSION

In this paper, an efficient CS-based algorithm is proposed within the MMV paradigm to deal with the speckle noise removal problem. The regularization by the mixed $l_{2,1}$ norm is considered for the proposed optimization problem. The considered regularizer is weighted iteratively by the vector of variance calculated with the adopted VBJS method. Therefore, the solution of the convex optimization problem is performed using the ADMM algorithm. Experimental results, using raw complex-valued data, have shown the efficiency of the proposed algorithm in terms of speckle removing, high quality reconstruction, and reduced computational burden.

ACKNOWLEDGMENT

The author(s) declared no potential conflicts of interest with respect to the research, authorship, and/or publication of this article.

REFERENCES

1. Curlander, J. C. and R. N. McDonough, *Synthetic Aperture Radar*, Vol. 11, Wiley, New York, 1991.
2. Moreira, A., P. Prats-Iraola, M. Younis, G. Krieger, I. Hajnsek, and K. P. Papathanassiou, "A tutorial on synthetic aperture radar," *IEEE Geoscience and Remote Sensing Magazine*, Vol. 1, No. 1, 6–43, 2013.
3. Massonnet, D. and J. C. Souyris, *Imaging with Synthetic Aperture Radar*, EPFL Press, 2008.
4. Lee, J. S., "Digital image enhancement and noise filtering by use of local statistics," *IEEE Transactions on Pattern Analysis and Machine Intelligence*, Vol. 2, No. 2, 165–168, 1980.
5. Kuan, D. T., A. A. Sawchuk, T. C. Strand, and P. Chavel, "Adaptive noise smoothing filter for images with signal-dependent noise," *IEEE Transactions on Pattern Analysis and Machine Intelligence*, Vol. 7, No. 2, 165–177, 1985.
6. Frost, V. S., J. A. Stiles, K. S. Shanmugan, and J. C. Holtzman, "A model for radar images and its application to adaptive digital filtering of multiplicative noise," *IEEE Transactions on Pattern Analysis and Machine Intelligence*, Vol. 4, No. 2, 157–166, 1982.
7. Lopes, A., R. Touzi, and E. Nezry, "Adaptive speckle filters and scene heterogeneity," *IEEE Transactions on Geoscience and Remote Sensing*, Vol. 28, No. 6, 992–1000, 1990.
8. Lopes, A., E. Nezry, R. Touzi, and H. Laur, "Structure detection and statistical adaptive speckle filtering in SAR images," *International Journal of Remote Sensing*, Vol. 14, No. 9, 1735–1758, 1993.
9. Bioucas-Dias, J. M. and M. A. Figueiredo, "Multiplicative noise removal using variable splitting and constrained optimization," *IEEE Transactions on Image Processing*, Vol. 19, No. 7, 1720–1730, 2010.
10. Xu, B., Y. Cui, Z. Li, B. Zuo, J. Yang, and J. Song, "Patch ordering-based SAR image despeckling via transform-domain filtering," *IEEE Journal of Selected Topics in Applied Earth Observations and Remote Sensing*, Vol. 8, No. 4, 1682–1695, 2014.
11. Sabanci, K., E. Yigit, A. Toktas, and A. Kayabasi, "A Hue-domain filtering technique for enhancing spatial sampled compressed sensing-based SAR images," *IET Radar, Sonar & Navigation*, Vol. 13, No. 3, 357–367, 2019.
12. Ozcan, C., B. Sen, and F. Nar, "Sparsity-driven despeckling for SAR images," *IEEE Geoscience and Remote Sensing Letters*, Vol. 13, No. 1, 115–119, 2015.
13. Feng, W., G. Nico, and M. Sato, "GB-SAR interferometry based on dimension-reduced compressive sensing and multiple measurement vectors model," *IEEE Geoscience and Remote Sensing Letters*, Vol. 16, No. 1, 70–74, 2018.
14. Borcea, L. and I. Kocyigit, "A multiple measurement vector approach to synthetic aperture radar imaging," *SIAM Journal on Imaging Sciences*, Vol. 11, No. 1, 770–801, 2018.
15. Potter, L. C., E. Ertin, J. T. Parker, and M. Cetin, "Sparsity and compressed sensing in radar imaging," *Proceedings of the IEEE*, Vol. 98, No. 6, 1006–1020, 2010.

16. Liu, S., J. Zhang, J. Liu, and Q. Yin, "$l_{1/2,1}$ group sparse regularization for compressive sensing," *Signal, Image and Video Processing*, Vol. 10, No. 5, 861–868, 2016.
17. Scarnati, T. and A. Gelb, "Accelerated variance based joint sparsity recovery of images from fourier data," *arXiv preprint arXiv:1910.08391*, 2019.
18. Gelb, A. and T. Scarnati, "Reducing effects of bad data using variance based joint sparsity recovery," *Journal of Scientific Computing*, Vol. 78, No. 1, 94–120, 2019.
19. Güven, H. E., A. Güngör, and M. Cetin, "An augmented Lagrangian method for complex-valued compressed SAR imaging," *IEEE Transactions on Computational Imaging*, Vol. 2, No. 3, 235–250, 2016.
20. Candes, E. J., M. B. Wakin, and S. P. Boyd, "Enhancing sparsity by reweighted l_1 minimization," *Journal of Fourier Analysis and Applications*, Vol. 14, No. 5, 877–905, 2008.
21. Giles, D., "The majorization minimization principle and some applications in convex optimization," Thesis, 2015, doi: 10.15760/honors.175.
22. Archibald, R., A. Gelb, and R. B. Platte, "Image reconstruction from undersampled Fourier data using the polynomial annihilation transform," *Journal of Scientific Computing*, Vol. 67, No. 2, 432–452, 2016.
23. Wang, Y., J. Yang, W. Yin, and Y. Zhang, "A new alternating minimization algorithm for total variation image reconstruction," *SIAM Journal on Imaging Sciences*, Vol. 1, No. 3, 248–272, 2008.
24. Duersch, M. I. and D. G. Long, "Analysis of time-domain back-projection for stripmap SAR," *International Journal of Remote Sensing*, Vol. 36, No. 8, 2010–2036, 2015.
25. Ponmani, E. and P. Saravanan, "Image denoising and despeckling methods for SAR images to improve image enhancement performance: A survey," *Multimedia Tools and Applications*, Vol. 80, No. 17, 26547–26569, 2021.
26. Yigit, E., S. Demirci, C. Ozdemir, and M. Tekbas, "Short-range ground-based synthetic aperture radar imaging: Performance comparison between frequency-wavenumber migration and back-projection algorithms," *Journal of Applied Remote Sensing*, Vol. 7, 073483, 2013.